CHEMISTRY OF MATERIALS

pubs.acs.org/cm

Article

Programmatically Regulating Morphological Evolution of Inert Polymeric Hydrogels Using Anchored Large-Deformable Muscle

Yu Peng,[#] Kaihang Zhang,[#] Baoyi Wu,[*] Jianlei Lu, Yukun Jian, Yaoting Xue, Xuxu Yang, Jiawei Zhang,[*] and Tao Chen[*]

Cite This: *Chem. Mater.* 2022, 34, 6582−6592

Read Online

ACCESS | Metrics & More | Article Recommendations | Supporting Information

ABSTRACT: Living organisms can generate diverse three-dimensional (3D) morphologies and programmatically regulate their morphological evolution via the neurally controlled expansion and contraction of soft tissues. Although polymeric hydrogels have been regarded as an ideal experimental platform for biomimetic morphing due to their soft-tissue-like properties, it is still a tricky problem to quantitatively design their 3D morphological evolution, especially for inert polymeric hydrogels. In this study, we developed a muscle-inspired deformation system that could programmatically regulate the morphological evolution of undeformable inert polymeric hydrogels using large-deformable hydrogels as muscles, which contained smart poly *N*-isopropylacrylamide (PNIPAm) microgel and could be anchored onto any hydrogels via interfacial diffusion polymerization (IDP). Moreover, by programmatically regulating the anchoring position of the large-deformable muscle, the 3D morphology of kirigami-shaped hydrogels could further evolve to obtain a more complex 3D morphology. Surprisingly, when the inert hydrogel was replaced by a shape-memory hydrogel, the 3D morphologies could be fixed and preserved for more than 1 month without any stress relaxation or swelling, even after removing the hydrogel muscle or external stimuli. Therefore, we believe that this deformation strategy will enhance our understanding of the life evolution of natural soft-wet organisms for developing intelligent soft materials such as shape-memory hydrogels, programmable deformations, and 3D biomimetic devices.

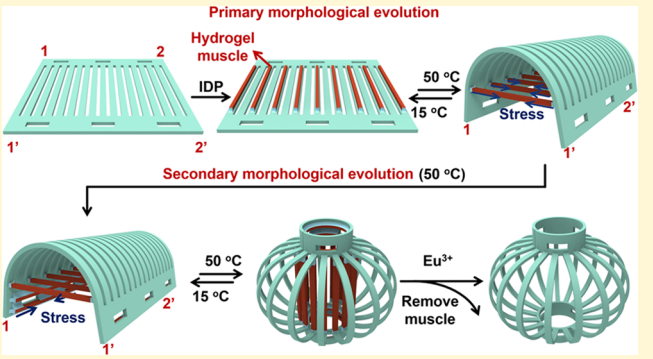

1. INTRODUCTION

For the purpose of preying, warning, and breeding, living organisms have evolved diverse three-dimensional (3D) morphologies and fantastic deformability that can consciously transfer their 3D morphologies via the neurally controlled expansion and contraction of soft tissues. This motivates several researchers to explore and imitate biomimetic deformation behavior for developing intelligent materials, flexible actuators, and soft robotics.[1−5] Because of the soft and wet properties of soft tissues, polymeric hydrogels have been regarded as an ideal experimental platform for bionics[6−10] and have thus received considerable interest for achieving programmed 3D morphologies.[11−14] Inspired by the biological morphologies, the potential capability of stimuli-responsive polymeric hydrogels to generate reversible deformability under external stimuli has been demonstrated.[15−18] Moreover, various anisotropic structures with alternative strategies were used to achieve bilayer,[19,20] pattern,[21,22] orientation,[23,24] and gradient composite[25,26] hydrogels with a programmed 3D morphology, which revealed the understanding of working principles in living organisms.[27,28]

Despite the significant efforts and development of deformable polymeric hydrogels, a considerable gap remains between the deformable polymeric hydrogel and the natural deformation system. In particular, the ability to spatially and temporally control the deformation process is limited by the inertness of the polymeric network.[29] For example, the expected 3D morphology was determined by the nondynamic anisotropic structure fabricated during preparation, and the number of corresponding configurations was also limited.[30,31] This limitation arises from the nondynamic polymeric network, discontinuous deformation process, and lack of control units to transfer the shape-morphing process in a timely manner. In contrast, octopus arms could exhibit various types of deformations or casually suspend the deformation process to adapt to changes in the external environment.[32] These continuously deforming motions are commonly observed in living organisms but are challenging to replicate in the inert polymeric hydrogel with an unchangeable structure and stable

Received: May 17, 2022
Revised: June 28, 2022
Published: July 15, 2022

Scheme 1. Muscle-Inspired Regulation of the Morphological Evolution of Inert Hydrogel[a]

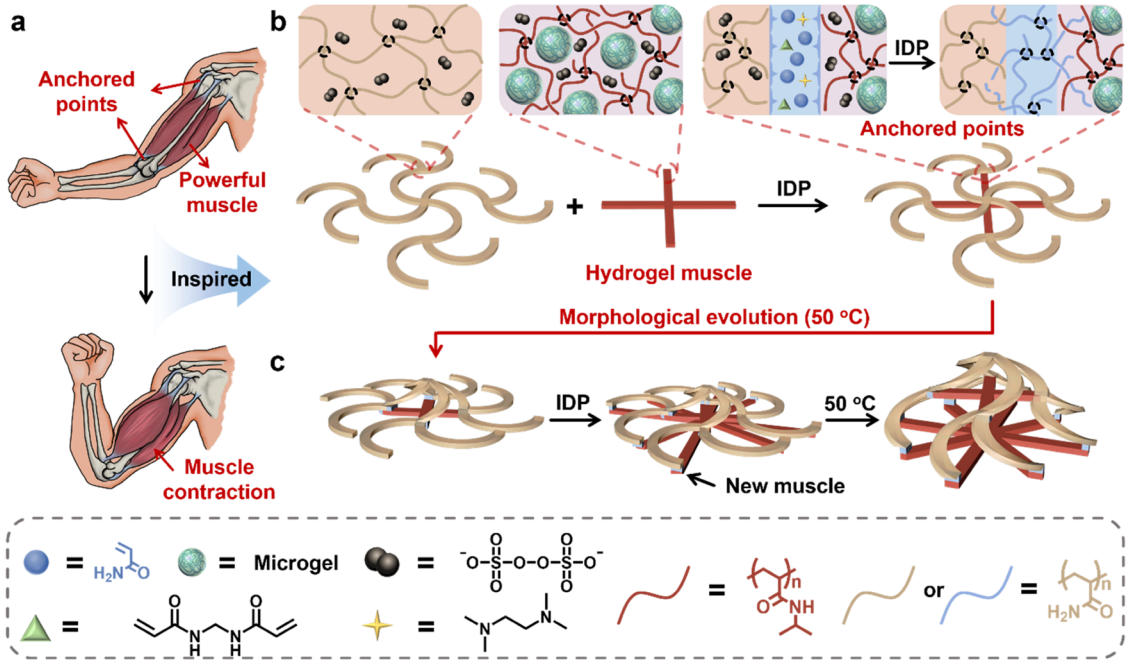

[a](a) Schematic illustration of muscle-actuated biomimetic morphing. A powerful muscle was anchored onto the sides of a bone via a tendon and an actuated elbow bending via muscle contraction. (b) Schematic illustration showing the muscle assembly process. The PNIPAm hydrogel was utilized as the hydrogel muscle to anchor onto the surface of the inserted hydrogel via IDP. (c) Schematic illustration of the 3D morphological evolution process. A freestanding 3D morphological hydrogel was obtained via the thermoresponsive contraction of an anchored hydrogel muscle. Furthermore, the primary 3D morphology of the hydrogel could evolve to a higher level of 3D morphology when anchoring a new hydrogel muscle.

chemical properties. Therefore, a universal strategy capable of programmatically regulating the morphological evolution of inert polymeric hydrogels could enhance the understanding of living organisms, complementing existing biomimetic morphing methods.

Human deformation systems containing inert rigid bones and soft muscles could generate various morphologies via the shrinking of powerful muscles (Scheme 1a), which inspired us to construct an external hydrogel muscle to assist and control the deformation of inert polymeric hydrogels.[33−35] In the practice of artificial muscles, because of the excellent volume phase transition behavior, poly *N*-isopropylacrylamide (PNIPAm) has garnered widespread interest in stimuli-responsive polymers and hydrogel actuators.[36] Although ordinary PNIPAm hydrogels have been utilized as hydrogel muscles to fabricate anisotropic hydrogel actuators and generate complex deformation,[37−39] the deswelling property (deswelling to 80% of the initial volume) is too poor to be compared with body muscles. Many strategies have been proposed to improve the deswelling property, such as decreasing the volume of the hydrogel bulk[40,41] and adding porogen,[42,43] but there is still a gap between the improvement and the ideal goal. Therefore, preparing a hydrogel muscle with powerful deformability to assist the deformation of inert undeformable polymeric hydrogels is an urgent priority.

Here, inspired by the muscle-actuated biomimetic morphing process, a thermoresponsive PNIPAm hydrogel loaded with the PNIPAm microgel was applied as the artificial muscle and anchored onto the surface of the inert hydrogel via interfacial diffusion polymerization (IDP) (Scheme 1b).[44] Because of the dynamic water channels provided by PNIPAm microgels, the hydrogel muscle exhibited large deformability (deswelling to 10% of the initial volume) and generated more mechanical energy than the ordinary PNIPAm hydrogel, inducing the shape-morphing of the inert hydrogel from a flat two-dimensional (2D) to a 3D morphology. Moreover, the deformed hydrogel could further evolve to a more complex 3D morphology by anchoring new hydrogel muscles in the appropriate position (Scheme 1c). In addition, when the inert hydrogels were replaced by a shape-memory hydrogel, the 3D morphology during the evolution process could also be fixed in a timely manner via the metal−ligand coordination between the alginate and metal ions such as Fe^{3+} and Eu^{3+}. Therefore, the expected that the 3D morphologies could be maintained long after removing the external stimulus. We believe that this work may provide new insights into the design and fabrication of deformable materials and devices.

2. EXPERIMENTAL SECTION

2.1. Materials. *N*-Isopropyl acrylamide (NIPAm, 98%), acrylamide (AAm, 98%), *N*,*N*,*N*′,*N*′-tetramethylethylenediamine (TEMED, 99%), ferric chloride ($FeCl_3$), sodium alginate (Alg), *N*,*N*′-methylenebisacrylamide (BIS, ≥98%), europium(III) nitrate hydrate ($Eu(NO_3)_3$, and 2,2′-azobis-2-methyl-propanimidamide (AAPH) were purchased from Aladdin Chemistry Co., Ltd. Ammonium peroxodisulfate (APS) was purchased from Sinopharm Chemical Reagent Co., Ltd. Poly(methyl methacrylate) (PMMA) microgel with a size of 500 nm was purchased from Lianlianfa Plastic Chemicals Co., Ltd.

2.2. Measurements. Ultraviolet−visible (UV−vis) absorption and transmittance spectra were acquired using a Perkin-Elmer LAMBDA 950 UV/Vis/NIR spectrophotometer. Digital photos of the materials were obtained by a smartphone camera (Huawei nova 5 pro), and those of the fluorescent materials were obtained under a UV lamp (ZF-5, 8 W, 365 nm). The maximum output force of the

https://doi.org/10.1021/acs.chemmater.2c01486
Chem. Mater. 2022, 34, 6582−6592

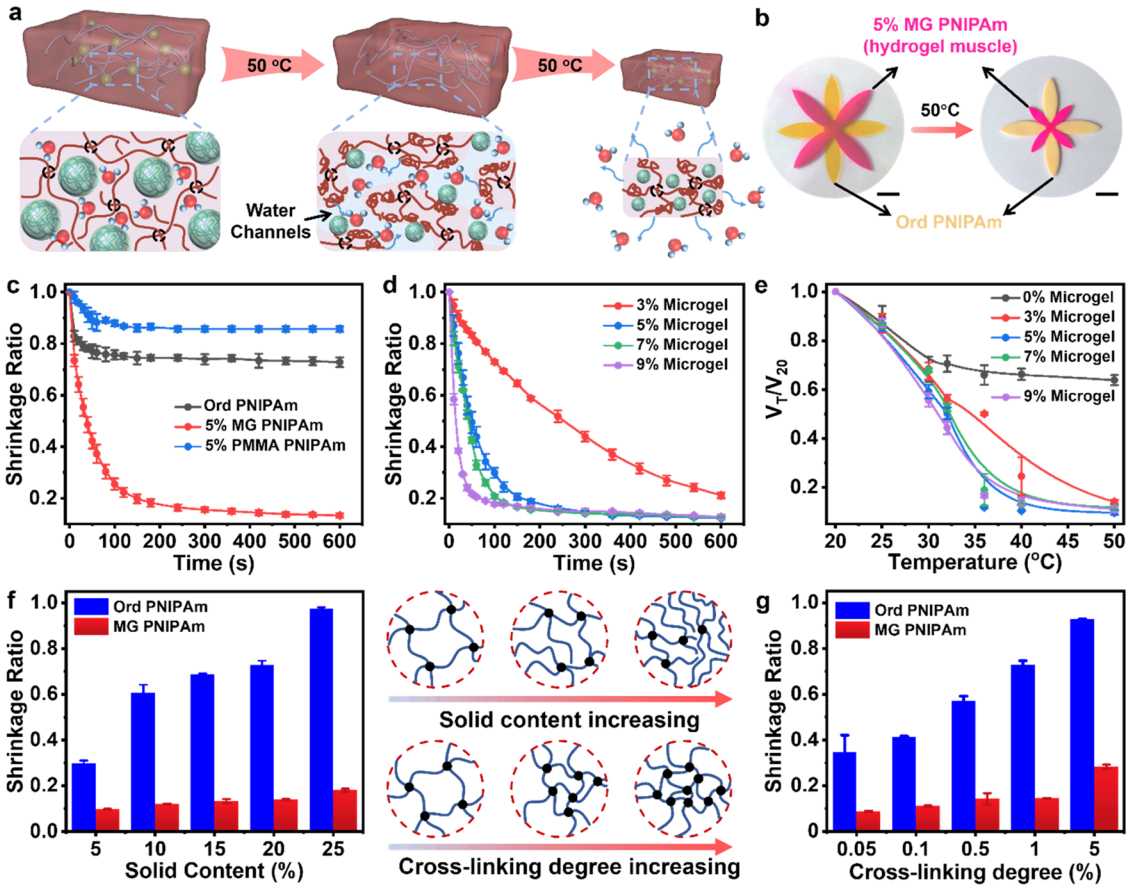

Figure 1. Large-scale deformation and deformation mechanism of MG PNIPAm hydrogels. (a) Large-scale deformation mechanism of the MG PNIPAm hydrogel. The PNIPAm microgel inside the MG PNIPAm hydrogel would generate plenty of water channels in water at 50 °C, facilitating water drainage and reducing the large deformability of the MG hydrogel. (b) Images showing the deformability of the MG PNIPAm hydrogel and ordinary PNIPAm hydrogel. (c) Kinetic shrinkage curve of the ordinary PNIPAm, MG PNIPAm hydrogel with 5% PNIPAm microgels, and MG PNIPAm hydrogel with 5% PMMA microgels. (d) Kinetic shrinkage curve of the MG PNIPAm hydrogel with different concentrations of PNIPAm microgels. (e) Dependence of the shrinkage ratio on different concentrations of PNIPAm microgels as a function of temperature. (f) Effect of the solid content on the shrinkage ratio of the ordinary PNIPAm hydrogel and the MG PNIPAm hydrogel. (g) Effect of the cross-linking degree on the shrinkage ratio of the ordinary PNIPAm hydrogel and the MG PNIPAm hydrogel. Scale bars: 1 cm.

PNIPAm hydrogel was measured using an electronic balance (METTLER TOLEDO ME204).

2.3. Synthesis of PNIPAm Microgel. First, 200 mL of pure water in a round-bottom flask was bubbled with N_2 gas for 5 min to remove the dissolved oxygen. Then, 2.545 g of NIPAm and 0.387 g of BIS were added to the water and stirred with a magnetic bar at 70 °C for 1 h. The flask was sealed, and the N_2 gas was blown into the flask below the liquid level. Next, 0.1145 g of AAPH was added to the solution. The polymerization was performed for 60 min at 70 °C, with a stirring of about 600 r.p.m. The microgel dispersion was immediately cooled in an ice-water bath, and the polymerization was terminated. The prepared gel particles were freeze-dried (DGJ-10C, Shanghai Boden) for subsequent use. The hydrodynamic diameters of the microgel in water at temperatures of 15 and 50 °C were measured by dynamic light scattering (Zetasizer Nano ZS, Malvern). Before each data collection, the microgel was highly diluted in deionized water.

2.4. Preparation of Hydrogel. In a typical experiment, the NIPAm monomer (0.6 g), PNIPAm microgel (0.2 g), BIS (6 mg), and APS (6 mg) were dissolved in 4 mL of deionized water and stirred to form a solution. Then, TEMED (4 μL) was added to the solution and transferred into a homemade mold, including two pieces of glass (2 mm) slides and one hollow silicone rubber sheet (1 mm) (similar to the image in Figure S3). The MG PNIPAm hydrogel was obtained after 12 h at 15 °C. PNIPAm hydrogel samples with various compositions (see Table S1 for the detailed feed formula) were synthesized by a similar procedure by varying the feed concentration of the PNIPAm microgel.

The NIPAm monomer (0.8 g), BIS (8 mg), and APS(8 mg) were dissolved in 4 mL of deionized water and stirred into a solution. Then, TEMED (4 μL) was added to the solution and transferred into the homemade mold, including two pieces of glass (2 mm) slides and one hollow silicone rubber sheet (1 mm). The ordinary PNIPAm hydrogel was obtained after 12 h at 15 °C.

AAm (0.71 g), BIS (21 mg), APS (21 mg), and alginate (2 wt %,10 g) were stirred together to form a solution. Then, TEMED (20 μL) was added to the solution and transferred into the homemade mold. The PAAm/alginate hydrogel was obtained after being placed vertically for 12 h at room temperature.

2.5. Preparation of Touch-Responsive Compound Hydrogel. A certain amount of as-prepared PAAm hydrogels was immersed into APS solution (15 mg/mL) for 5 min and then transferred and allowed to set in a homemade mold; then, a mixture of the PNIPAm hydrogel precursor containing the NIPAm monomer (0.6 g), BIS (6 mg), PNIPAm microgel (0.2 g), TEMED (150 μL), and deionized water (4 mL) was poured into the gaps of the PAAm hydrogels. The compound hydrogel was obtained after 6 h at room temperature.

2.6. Preparation of 3D Morphology of As-Prepared Hydrogel. The as-prepared PAAm hydrogel and MG PNIPAm hydrogel were immersed in APS (15 mg/mL) for 5 min. Then, 2.13 g of the AAm monomer, 21 mg of BIS, and 150 μL of TEMED were added to 10 mL of alginate solution (2%) to prepare the hydrogel precursor. Subsequently, the MG PNIPAm hydrogel was placed onto the surface

https://doi.org/10.1021/acs.chemmater.2c01486
Chem. Mater. 2022, 34, 6582−6592

of PAAm and the hydrogel precursor was added to the expected anchor point. The MG PNIPAm hydrogel would be anchored after 5 min.

2.7. Characterizations of PNIPAm Gels. Dynamic thermoresponsive shrinkage behaviors of hydrogels were measured by recording videos of the volume-change processes using a digital camera (Huawei nova 5 pro) after the environmental temperature was abruptly increased from 15 to 50 °C. After reaching equilibrium in cold water at 15 °C for 48 h, the hydrogel sample was suddenly transferred from the cold water at 15 °C to hot water at 50 °C. At the same time, the video recording was started. The size of the hydrogel was measured using digital images obtained from the movies. The shrinkage ratio of a hydrogel is defined as V_t/V_0 as a function of time, in which V_0 and V_t are the volumes of the hydrogel sample at the beginning and at time t, respectively.

To investigate the temperature dependence of the equilibrium volume phase transition, MG PNIPAm and ordinary PNIPAm were cut into square with a length of 20 mm. The container was placed in a thermostatic water bath with a temperature fluctuation of ±0.1 °C. The equilibrium volumes of hydrogels at selected temperatures were recorded from 20 to 50 °C. As the LCST of PNIPAm is 32 °C, the test temperature range was selected to cross the LCST. The equilibrium volumes of hydrogels at selected temperatures were recorded at each temperature; the temperature was maintained constant for 30 min to ensure that the hydrogel samples had reached the equilibrium state before measurement. The side length of hydrogels was recorded by a digital camera and surveyed. The equilibrium swelling ratio at T °C is defined as V_T/V_{50}, where V_T and V_{50} are the equilibrium volumes of the hydrogel at temperature T and 50 °C, respectively.

3. RESULTS AND DISCUSSION

In general, when an ordinary PNIPAm hydrogel bulk is placed in a hot environment, because of the 3D structure, the surface temperature usually reaches the volume phase transition temperature (VPTT). Thus, at the beginning of the deswelling process, the surface of the PNIPAm hydrogel bulk is hydrophobic, whereas the interior is still hydrophilic. The hydrophobic surface will hinder the transfer of water from the interior to the external environment, which leads to a poor deswelling property. According to the Tanaka−Fillmore theory, the diffusion rate of water in the hydrogel is inversely proportional to the square of the hydrogel dimension, which indicates that the deswelling property will be enhanced by decreasing the volume.[41] Therefore, balancing the hydrogel size and the deswelling property remains a challenge.

In this study, we proposed a feasible strategy to prepare a macrohydrogel by introducing the microgel into the macrohydrogel network, which induced large deformability. Thus, we first fabricated the PNIPAm microgels with a narrow size distribution with reference to a previous study (Figure S1).[45] As shown in Figure S2, the average hydrodynamic diameter of PNIPAm microgels was ∼530 nm at 15 °C, and it decreased to ∼260 nm at 50 °C due to the volume phase transition of PNIPAm chains. Subsequently, the prepared PNIPAm microgels were introduced into the PNIPAm hydrogel network (Figure S3). When the PNIPAm hydrogel-containing PNIPAm microgels (MG PNIPAm) were immersed in water at 50 °C, the large-scale collapse of internal PNIPAm microgels generated plenty of water channels (Figure 1a). Therefore, the internal water could be more easily drained out, and the PNIPAm hydrogel bulk could deswell to a smaller volume (Figure 1b). The shrinkage ratio of the MG PNIPAm hydrogel was ∼0.1, whereas that of the ordinary PNIPAm hydrogel was ∼0.7.

To prove the importance of the dynamic water channels in the deswelling process, nonresponsive microgels (PMMA microgels) of the same size were introduced into the PNIPAm hydrogel as a control group. When the PNIPAm hydrogel-containing PMMA microgels were immersed in water at 50 °C, the shrinkage ratio was ∼0.84 (Figure 1c), indicating that the generation of water channels played a major role in the deswelling process. Moreover, different concentrations of the PNIPAm microgel were introduced into the hydrogel to evaluate the influence of PNIPAm microgels (Table S1). As shown in Figure 1d, with an increase in the concentration of PNIPAm microgels, more water channels would be generated, and each independent water channel tended to be connected to form a water-channel network. Thus, both the shrinkage ratio and the shrinkage speed would increase. Besides, if a stronger external energy (higher temperature) was applied, the internal water could also be drained and it increases the deswelling property. Similarly, with an increased concentration of PNIPAm microgels, the lowest critical temperature of the lowest shrinkage ratio decreased, which means that the internal water was easier to drain (Figure 1e).

As mentioned above, the hydrophobic surface of the hydrogel bulk would hinder the internal water-draining process. Therefore, a denser hydrogel network would delay the deswelling process. We changed the network density of PNIPAm hydrogels by varying the content of monomers and cross-linkers. As shown in Figure 1f, when the solid content of the ordinary PNIPAm hydrogel was 25%, the shrinkage ratio was ∼0.97. However, the shrinkage ratio would decrease to 0.3 when the solid content decreased to 5%. As a comparison, there was a slight increase in the shrinkage ratio of MG PNIPAm hydrogels with an increase in the solid content. This indicated that improving the deswelling property via dynamic water channels was efficient. Similarly, when the cross-linking degree decreased from 5 to 0.05%, the shrinkage ratio of the ordinary hydrogel decreased from 0.92 to 0.32, and the MG hydrogel still exhibited excellent deswelling property (Figure 1g).

Besides, this theory may still be appropriate for other external stimuli. For example, when the ordinary PNIPAm hydrogel and the MG PNIPAm hydrogel were immersed in ethanol, respectively, although the PNIPAm hydrogel did shrink because of its poor solubility in ethanol, the shrinkage ratios of both the groups were still similar to the value of the condition where the ordinary PNIPAm hydrogel swelled in water at 50 °C. In contrast, when the two groups were evaluated with 20% ethanol in water, the MG PNIPAm hydrogel could exhibit a large-scale swelling property, whereas the shrinkage ratio of the ordinary PNIPAm hydrogel was still poor (Figure S4). This phenomenon indicated that the dynamic water channels played an important role in the draining process in a water environment.

Traditional stimuli-responsive hydrogels could transform the external energy into mechanical energy via the deswelling process. Thus, it has been regarded as an ideal candidate for artificial muscle.[24,46,47] Compared with ordinary PNIPAm hydrogels, MG PNIPAm hydrogels could yield an output tensile force of up to ∼0.07 mN with the deswelling process. In contrast, the ordinary PNIPAm hydrogel could yield a maximum tensile strength of only ∼0.02 mN due to its poor deswelling property (Figure S5). Besides, the large-scale deformation of MG hydrogels indicates that they can export more mechanical energy. According to the formula, $W = F \times S$,

https://doi.org/10.1021/acs.chemmater.2c01486
Chem. Mater. 2022, 34, 6582−6592

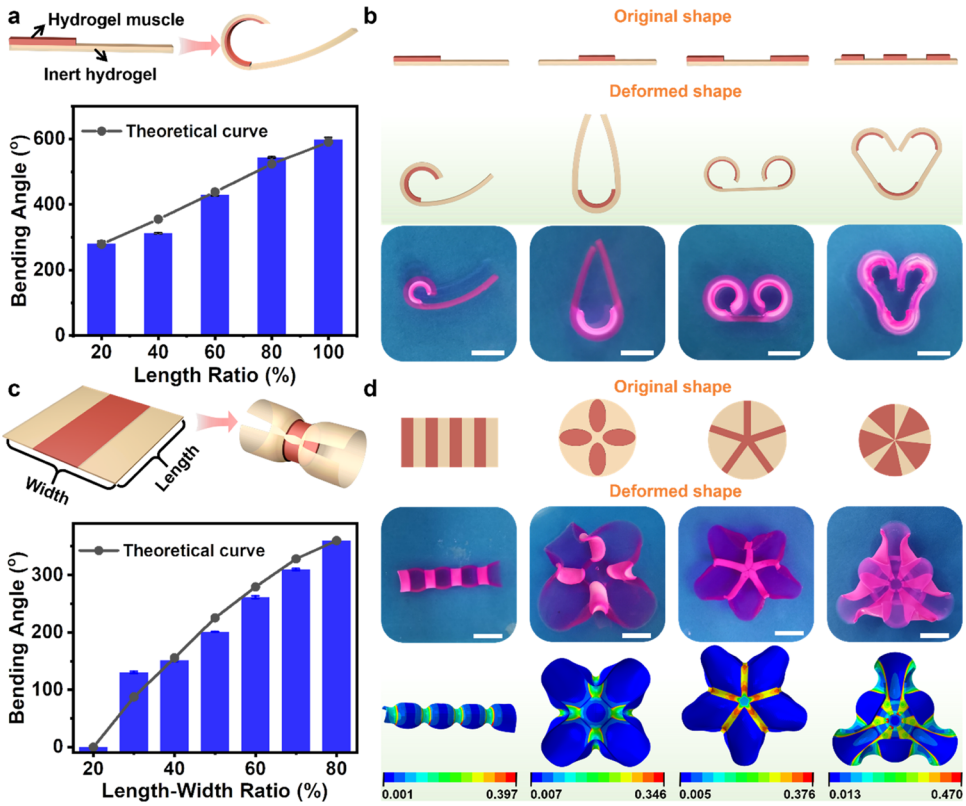

Figure 2. 3D programmed deformation from 1D and 2D hydrogels. (a) Theory and experiment showing the bending angle as a function of the length ratio of the composite hydrogel. (b) Programmed deformation of the composite hydrogel from 1D to 2D. (c) Theory and experiment showing the bending angle as a function of the length:width ratio of the composite hydrogel. (d) Programmed deformation of the composite hydrogel from 2D to 3D. All of the above hydrogels were deformed in water at 50 °C for 5 min. Scale bars: 1 cm.

where F represents the exported tensile force and S represents the displacement, the export mechanical energy of MG hydrogel is 0.52 J/kg, which is much higher than that of the ordinary PNIPAm hydrogel (0.15 J/Kg) (Figure S6, Movie S1).

Benefitting from the excellent deswelling property, the MG PNIPAm hydrogels could exhibit large-scale deformability and endowed the anisotropic hydrogel actuators with a potent actuating property. Here, we used a bilayer hydrogel actuator as an example. As shown in Figure 2a, the PAAm hydrogel layer was polymerized. Subsequently, before completely curing, the MG PNIPAm hydrogel layer with different lengths was polymerized onto the PAAm hydrogel surface to form a bilayer structure.[20,48] Due to the anisotropic deswelling of the bilayer structure, the bilayer hydrogel actuator could bend from the strip form to a circle. According to the finite element modeling, the bilayer hydrogel actuator-containing microgel could turn by ~600° for the large-scale deswelling of the MG PNIPAm hydrogel in 5 min and recover to the initial shape in 60 min when transferred to water at 15 °C (Figure S8). Even when the length ratio decreased to 20% (Figure S7), the hydrogel actuator could bend to 280°. It indicated that a small piece of the MG PNIPAm hydrogel could adjust the morphology of the inert hydrogel in a large dimension. For instance, when an MG hydrogel with a length ratio of 30% was attached to the middle area of the inert hydrogel, the obtained hydrogel actuator could form a teardrop shape from the strip in water at 50 °C. Similarly, by controlling the position and length ratio of the MG hydrogel, a more complex 2D morphology such as a heart shape could be obtained in the same way (Figure 2b).

By anchoring the inert hydrogel onto the surface of the MG PNIPAm hydrogel, a composite hydrogel with complex 3D deformation functions can be fabricated. As shown in Figure 2c, we prepared a flat hydrogel containing the MG PNIPAm hydrogel in the middle area and the inert hydrogel in the remaining area, and then, immersed it in water at 50 °C. Because of the deswelling of the MG hydrogel, bending stress is concentrated in the middle part, causing the flat hydrogel to curl. The MG PNIPAm hydrogel ratio and the length:width ratio of the hydrogel strips were varied to evaluate their influences on the deformation degree θ (Figure S9, Figure S10). As shown in Figure S11, when the MG PNIPAm hydrogel content is low, the stress generated by the MG PNIPAm hydrogel is too weak to actuate the whole hydrogel. Thus, the value of θ is small. With an increase in the ratio of the MG PNIPAm hydrogel, the compressive stress along the boundary between the MG PNIPAm hydrogel and the inert hydrogel would increase, which exacerbates the bending of the whole hydrogel. The bending angle reaches the maximum when the ratio reaches 40%. Besides, the length:width ratio influences the deformation process when the MG hydrogel ratio is constant. The value of θ increased with the length:width ratio, which was consistent with the result provided by the finite element modeling.

Based on the basic model presented above, more 2D patterns could be designed in the flat hydrogel, which could deform into the expected 3D bio-inspired morphology similar to living organisms such as orchid petals and jellyfish (Figure 2d). It is worth mentioning that the critical mechanism of forming the 3D morphology is severe stress in the interface.

https://doi.org/10.1021/acs.chemmater.2c01486
Chem. Mater. 2022, 34, 6582−6592

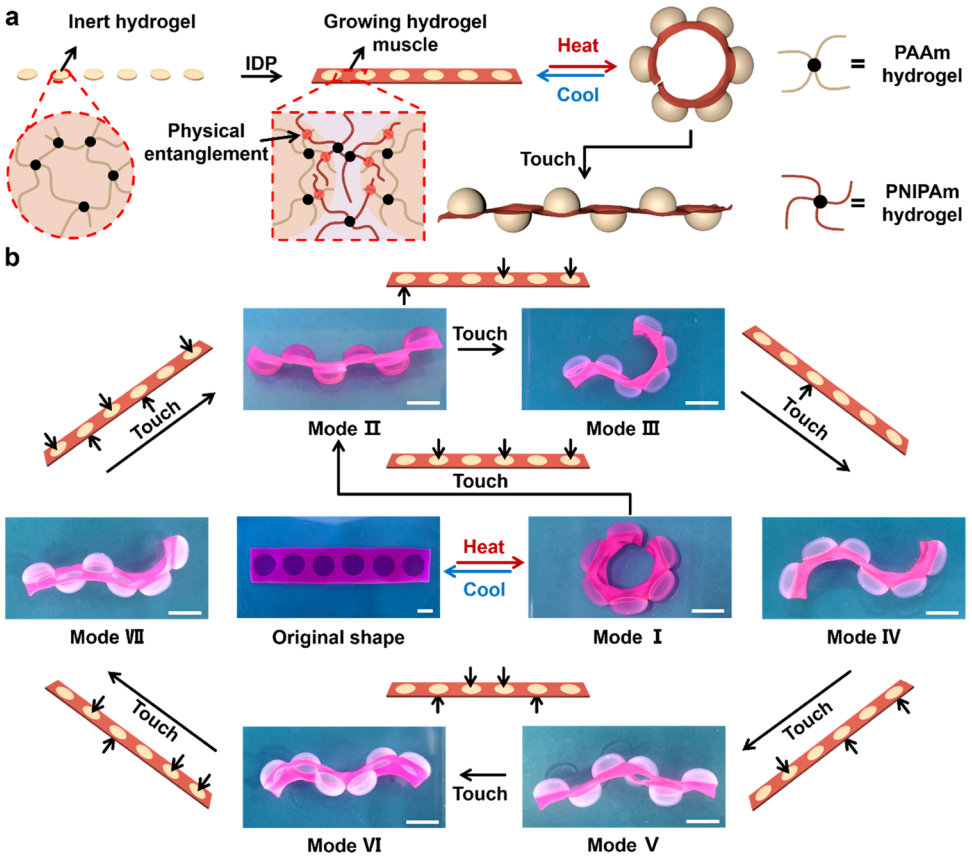

Figure 3. Morphological evolution based on touch-responsive hydrogels. (a) Schematic illustration of the fabrication and deformation mechanism of touch-responsive hydrogels. A composite flat hydrogel was prepared by growing hydrogel muscle in the gaps between the arranged hydrogels. With the large-scale contraction of the hydrogel muscle in water at 50 °C, the hybrid flat hydrogel would deform into a 3D dome shape. (b) Multiple morphologies of touch-responsive hydrogels. When the composite flat hydrogel comes in contact with an external force during the thermo-triggered deformation process, diverse 3D morphologies would be obtained and transformed. Scale bars: 1 cm.

Thus, if the ordinary PNIPAm hydrogel replaced the MG PNIPAm hydrogel, the corresponding 3D morphology could not be obtained due to the poor deswelling property (Figure S12).

Utilizing the MG PNIPAm hydrogel as a large-deformable building block, complex 3D structures can be fabricated. As shown in Figure 3a, some disk-shaped PAAm hydrogels containing ammonium persulfate (APS) were prepared and arranged. Subsequently, the hydrogel precursor contained in PNIPAm microgels was poured into the gaps of PAAm hydrogels and polymerized via interfacial diffusion polymerization (IDP). Due to the interpenetrating structure caused by IDP, the new MG PNIPAm hydrogel could grow firmly in the gaps between PAAm hydrogels, as indicated by the scanning electron microscope (SEM) images (Figure S13). When the composite flat hydrogel is immersed in water at 50 °C, a part of the MG PNIPAm hydrogel would deswell, and the accumulated stress in the interface between the MG PNIPAm hydrogel and the PAAm hydrogel would extrude the disk-shaped PAAm hydrogel to form a 3D dome shape. In theory, these disks with circumferential accumulated stress will undergo buckling, which is bistable, with an equal probability of forming an upward- or a downward-facing dome. Thus, when all of the disk-shaped PAAm hydrogels deformed in the same direction, the composite hydrogel could form a circular shape. Interestingly, when an external force comes in contact with the disk-shaped PAAm hydrogel during the deformation process, the current mechanically metastable state would be disturbed, and the hydrogel would deform in the opposite direction. As a result, one type of flat hydrogel could generate various 3D morphologies, and each morphology could be converted to the other by contact stimulus(Figure 3b).

As discussed above, with the help of the MG PNIPAm hydrogel, even inert hydrogels could be encoded and deformed to the programmed morphologies. Besides, the MG PNIPAm hydrogel could also be utilized as a deformable muscle to precisely control and fabricate stable 3D morphologies from the inert hydrogel. For example, as shown in Figure 4a, shape-memory hydrogels, PAAm/alginate hydrogel strips, were prepared as passive blocks. Afterward, an MG PNIPAm hydrogel strip, which functions as a hydrogel muscle, was placed on the surface of the as-prepared PAAm/alginate hydrogel, and both ends of the hydrogel strips were anchored via IDP to fabricate a composite hydrogel. When the composite hydrogel is immersed in water at 50 °C, the hydrogel muscle would shrink and generate shrinkage stress at the anchored points. Thus, PAAm/alginate hydrogel strips could deform into an arched shape. After adding metal ions and physically removing the MG PNIPAm hydrogels, the arched shape could be fixed via supramolecular interactions between alginate chains and metal ions.[49−51] It is worth noting that although the new gradient structure inside could not be removed, the final shape of the PAAm/alginate hydrogel would

https://doi.org/10.1021/acs.chemmater.2c01486
Chem. Mater. 2022, 34, 6582−6592

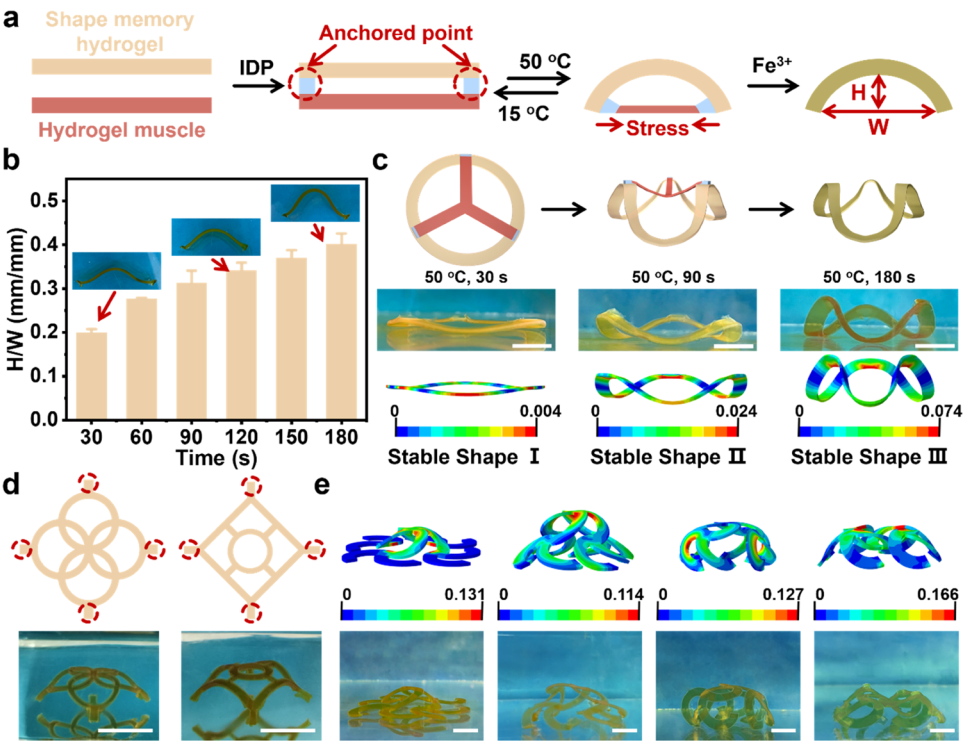

Figure 4. 3D morphological evolution process from 1D and 2D hydrogels. (a) Schematic illustration of the fabrication process of the 2D morphology from PAAm/alginate hydrogel strips. Both ends of the hydrogel muscle were anchored onto the surface of a shape-memory hydrogel via IDP. (b) Quantitative measurement of the shape-changing capability of the composite hydrogel. (c) 3D shape-changing capability of the composite hydrogel and programmatically controllable 3D morphology of the PAAm/alginate hydrogel ring. (d) Illustration and images showing the 3D morphology of the kirigami-shaped PAAm/alginate hydrogel. The hydrogel was deformed in water at 50 °C for 5 min, and the temporary shape was fixed by Fe^{3+}. (e) Illustration and images showing the 3D morphology of the PAAm/alginate hydrogel with a multitier configuration. The hydrogel was deformed in water at 50 °C for 5 min, and the temporary shape was fixed by Fe^{3+}. Scale bars: 1 cm.

not be influenced by the similar hydrogel composition between the new gradient structure and the initial hydrogel.

To quantitatively analyze the morphology of the as-prepared PAAm/alginate hydrogel during the deformation process, the characteristic shape parameter (RSP), which was defined as the ratio between the height and the width of the PAAm/alginate hydrogel, was utilized to describe the morphologies.[52,53] As shown in Figure 4b, because of the shrinkage of the hydrogel muscle, the width decreased, whereas the height increased, thereby increasing the RSP value from 0 to 0.53 in 5 min. Besides, the deformation process was reversible. When the synthesized hydrogel was transferred from 50 to 15 °C, it recovered the initial shape, with the RSP value decreasing to 0 in 60 min (Figure S14). During the deformation process, when the composite hydrogel was transferred to 0.1 M Fe^{3+} or a large amount of Fe^{3+} was added to the original solution, the transient shape of the PAAm/alginate hydrogel could also be fixed via the metal−ligand coordination between the alginate and Fe^{3+}. Therefore, according to the value of RSP, the morphological change of the PAAm/alginate hydrogel from 1D to 2D could be digitized, and the PAAm/alginate hydrogel with the expected deformation degree could be obtained.

Based on the above deformation model, when a three-armed hydrogel muscle was anchored to the surface of the ring-shaped PAAm/alginate hydrogel, the shrinkage stress generated in the hydrogel muscle led to pulling forces in the radial direction, which induced a wave-shaped surface from the flat surface (Figure 4c, Movie S2). Moreover, by controlling the deformation process, various morphologies with different deformation degrees would be obtained and maintained over a week without any elastic relaxation (Figure S15). Thus, the hydrogel muscle might be helpful for the construction of a hydrogel morphology with the allotype configuration. In contrast, if a ring-shaped MG PNIPAm hydrogel was anchored to the surface of the three-armed PAAm/alginate hydrogel, the 2D PAAm/alginate hydrogel could also be deformed to a 3D dome shape due to the shrinkage stress (Figure S16). Interestingly, irrespective of the shape of the deformable muscle, all of the 2D PAAm/alginate hydrogels could be deformed to the expected morphologies. For example, when a four-armed PAAm/alginate hydrogel was anchored to the surface of the flat MG PNIPAm, the isotropic shrinkage stress could also actuate the shape of the PAAm/alginate hydrogel to the 3D dome shape (Figure S17). In addition, more patterns of the 2D PAAm/alginate hydrogel, such as the kirigami shape, could be deformed to the corresponding 3D shape in the same way (Figure 4d).

Furthermore, the 3D morphologies of the deformed hydrogel could also be programmatically adjusted to form a multitier configuration via a multiple deformation process. As shown in Figure 4e, a four-armed hydrogel muscle was anchored onto the surface of the 2D kirigami-shaped PAAm/alginate hydrogel in the inner area. After immersing in water at 50 °C, the inner space of the hydrogel was first deformed to a 3D shape, whereas the outer area of the hydrogel remained flat. Subsequently, an eight-armed MG PNIPAm was further anchored to several points in the outer area (Scheme 1b,c). Therefore, the 3D-shaped hydrogel could be further deformed in the next stage. During the multiple deformation process,

https://doi.org/10.1021/acs.chemmater.2c01486
Chem. Mater. 2022, 34, 6582−6592

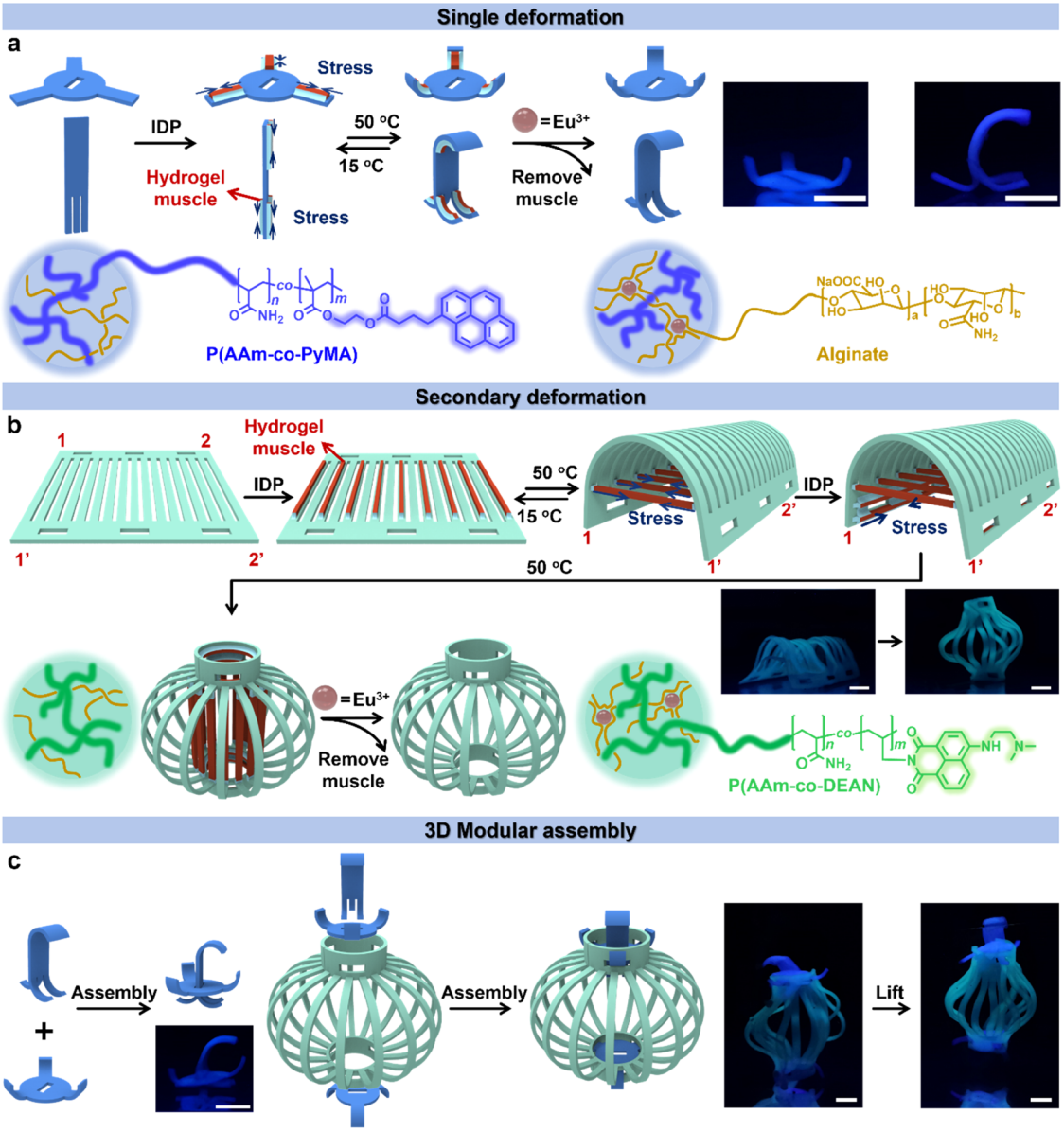

Figure 5. Programmable morphological evolution and 3D modular assembly of multicolor fluorescent hydrogels. (a) Single 3D deformation process of the blue fluorescent hydrogel. Some hydrogel muscles were anchored onto the surface of the as-prepared blue fluorescent hydrogel via IDP and actuated to a 3D morphology at 50 °C. After immersing in the Eu^{3+} solution and removing the hydrogel muscle, the blue fluorescent hydrogel with a 3D morphology was obtained. (b) Secondary deformation process of the green fluorescent hydrogel. Some hydrogel muscles were anchored onto the surface of the kirigami-shaped green fluorescent hydrogel via IDP and actuated to an arched shape. Subsequently, more new hydrogel muscles were programmatically anchored onto the surface of the arch-shaped hydrogel. Thus, the arch-shaped hydrogel would transfer to a 3D lantern shape in water at 50 °C. After immersing in Eu^{3+} solution and removing the hydrogel muscle, the green fluorescent hydrogel with a 3D lantern shape was obtained. (c) 3D modular assembly process of hydrogels. The deformed blue and green fluorescent hydrogels could be assembled to form a device by mechanical interlocking. Scale bars: 1 cm.

various multitier configurations could be generated by controlling the anchored position and sequence.

As mentioned above, the deformation approach may aid the inert hydrogel in forming 3D morphologies, which may also benefit their corresponding applications, such as the 3D modular assembly.[54] For instance, as shown in Figure 5a, the blue fluorescent polymer, poly(acrylamide-co-1-pyrenylmethyl acrylate) (P(AAm-co-PyMA)), was introduced into the PAAm/alginate hydrogel network to prepare a blue fluorescent hydrogel. Then, the blue fluorescent hydrogel was cut into a three-armed shaped and comb shape by a laser cutter, and many MG PNIPAm hydrogel strips were anchored to the relative areas via IDP. Due to the thermoresponsive behavior, the MG PNIPAm hydrogel strips generated a high amount of stress along the axial direction, thereby deforming to the 3D morphology. Finally, to preserve the fluorescent property, the coordinated metal ion was changed from Fe^{3+} to Eu^{3+}, and the 3D morphologies could be fixed via the metal−ligand coordination between the alginate and metal ions after removing the deformable muscle. However, in some types of shape-memory hydrogels, the above 3D morphology may also be obtained by deforming the hydrogel by hand and fixing the shape with a special mold. When the 3D morphology is more complex, or the deformation process involves multiple steps,

https://doi.org/10.1021/acs.chemmater.2c01486
Chem. Mater. 2022, 34, 6582−6592

the traditional method is inefficient, and a new approach to form the complex 3D morphology is necessary.

Similarly, as shown in Figure 5b, when the green fluorescent polymer, poly acrylamide-co-4-(*N*,*N*-dimethylaminoethylene) amino-*N*-allyl-1,8-naphthalimide (P(AAm-co-DEAN)), was introduced into the network of the PAAm/alginate hydrogel, a green fluorescent hydrogel was obtained. After cutting by a laser cutter, some MG PNIPAm hydrogel strips were also anchored into the axes of 11′ and 22′. Thus, the flat hydrogel could be deformed to a 3D arched shape. Subsequently, some new MG PNIPAm hydrogel strips were anchored into 12 and 1′2′ axes. When the deformed hydrogel was transferred back into hot water, the shrinkage of the MG PNIPAm hydrogel in the axes of 12 and 1′2′ could cause secondary deformation of the green fluorescent hydrogel from a 3D arched shape to a 3D lantern shape. At last, the 3D lantern shape of the green fluorescent hydrogel could be fixed in the same way and obtained after removing the MG PNIPAm hydrogel.

Benefiting from the programmable 3D morphology of hydrogels, the 3D modular assembly could be realized and applied to form higher-level structures. As shown in Figure 5c, the comb-shaped hydrogel could go through the hole reserved for the three-armed hydrogel. Due to the deformation of the comb-shaped hydrogel, the three-armed hydrogel could be firmly stuck in the middle of the deformed comb-shaped hydrogel. Furthermore, two three-armed hydrogels, a comb-shaped hydrogel, and a lantern-shaped hydrogel could also be assembled to form a complete device with a 3D morphology via the reserved hole. The assembled lantern-shaped hydrogel could maintain its structure via mechanical interlocking and could even be lifted. The 3D modular assembly may benefit many emerging fields such as multifluorescent hydrogels, structural hydrogels, and multifunctional soft robotics.

4. CONCLUSIONS

In summary, to overcome the challenge presented by the existing deformable polymeric hydrogel not being able to programmatically regulate the shape-morphing process, a muscle-inspired deformation system was proposed. In this system, the powerful hydrogel muscle (MG PNIPAm) with large-scale deformability (deswelling to 10% of the original volume) was prepared by introducing thermoresponsive PNIPAm microgels into the network of the PNIPAm hydrogel. With the interfacial diffusion polymerization (IDP) approach, hydrogel muscles could be firmly anchored onto the surface of any inert polymeric hydrogels and actuated to the programmed 3D morphologies. In addition, inert polymeric hydrogels could also evolve to more complex 3D morphologies by programmatically regulating the anchored position and the sequence of the hydrogel muscle via IDP. Furthermore, by utilizing the hydrogel muscle to deform a shape-memory hydrogel, the morphology and shape-morphing process could be instantly and precisely controlled, thus realizing the 3D modular assembly. This study provided new insights into the morphological regulation of polymeric hydrogels, complementing existing biomimetic morphing methods, which may enhance the understanding of working principles in living organisms and provide new opportunities for the development of deformable intelligent materials and devices.

■ ASSOCIATED CONTENT

Supporting Information

The Supporting Information is available free of charge at https://pubs.acs.org/doi/10.1021/acs.chemmater.2c01486.

Feed formula of the MG PNIPAm hydrogel; synthesis of the PNIPAm microgel; thermoresponsive hydrodynamic diameters of the PNIPAm microgel; preparation process of the MG PNIPAm hydrogel; deswelling property of the MG PNIPAm hydrogel in ethanol solution; maximum output force and mechanical energy export of hydrogels; complex deformation process; bending and recovery process of bilayer hydrogels; variation of bending angles of different MG PNIPAm hydrogel ratios; 3D deformation process of hydrogels composed of ordinary PNIPAm and PAAm; cross-sectional SEM images of the bilayer hydrogel; bending and recovery process of the synthesized hydrogel; durability of the deformed hydrogel after treating with Fe^{3+}; 3D deformation process of the compound hydrogels (PDF)

Deswelling property of the MG PNIPAm hydrogel and ordinary hydrogel (Movie S1) (MP4)

3D deformation process of the compound hydrogels (Movie S2) (MP4)

■ AUTHOR INFORMATION

Corresponding Authors

Baoyi Wu − *Key Laboratory of Marine Materials and Related Technologies, Zhejiang Key Laboratory of Marine Materials and Protective Technologies, Ningbo Institute of Material Technology and Engineering, Chinese Academy of Sciences, Ningbo 315201, China; School of Chemical Sciences, University of Chinese Academy of Sciences, Beijing 100049, China;* orcid.org/0000-0003-2878-6386; Email: wubaoyi@nimte.ac.cn

Jiawei Zhang − *Key Laboratory of Marine Materials and Related Technologies, Zhejiang Key Laboratory of Marine Materials and Protective Technologies, Ningbo Institute of Material Technology and Engineering, Chinese Academy of Sciences, Ningbo 315201, China; School of Chemical Sciences, University of Chinese Academy of Sciences, Beijing 100049, China;* orcid.org/0000-0002-3182-9239; Email: zjwmail163@163.com

Tao Chen − *Key Laboratory of Marine Materials and Related Technologies, Zhejiang Key Laboratory of Marine Materials and Protective Technologies, Ningbo Institute of Material Technology and Engineering, Chinese Academy of Sciences, Ningbo 315201, China; School of Chemical Sciences, University of Chinese Academy of Sciences, Beijing 100049, China;* orcid.org/0000-0001-9704-9545; Email: tao.chen@nimte.ac.cn

Authors

Yu Peng − *Key Laboratory of Marine Materials and Related Technologies, Zhejiang Key Laboratory of Marine Materials and Protective Technologies, Ningbo Institute of Material Technology and Engineering, Chinese Academy of Sciences, Ningbo 315201, China; School of Chemical Sciences, University of Chinese Academy of Sciences, Beijing 100049, China*

Kaihang Zhang − *Department of Engineering Mechanics, Zhejiang University, Hangzhou 310027, China*

Jianlei Lu − *School of Materials Science & Chemical Engineering, Ningbo University, Ningbo 315211, China*
Yukun Jian − *College of Chemical Engineering, Ningbo Polytechnic, Ningbo 315800, China*
Yaoting Xue − *Department of Engineering Mechanics, Zhejiang University, Hangzhou 310027, China*
Xuxu Yang − *Department of Engineering Mechanics, Zhejiang University, Hangzhou 310027, China;* orcid.org/0000-0003-2779-1618

Complete contact information is available at: https://pubs.acs.org/10.1021/acs.chemmater.2c01486

Author Contributions

#Y.P. and K.Z. contributed equally to this work. This manuscript was written through contributions of all authors. All authors gave approval to the final version of the manuscript.

Notes

The authors declare no competing financial interest.

■ ACKNOWLEDGMENTS

The authors thank Israt Ali from the Institute National de la Recherche Scientifique for his kind help with the revision of this manuscript. This work was supported by the National Natural Science Foundation of China (51873223), Zhejiang Provincial Natural Science Foundation of China (LD22E050008), the Sino-German mobility programme (M-0424), and K. C. Wong Education Foundation (GJTD-2019-13).

■ REFERENCES

(1) Zhao, Z. G.; Fang, R. C.; Rong, Q. F.; Liu, M. J. Bioinspired Nanocomposite Hydrogels with Highly Ordered Structures. *Adv. Mater.* **2017**, *29*, No. 1703045.
(2) Wei, S.; Lu, W.; Le, X.; Ma, C.; Lin, H.; Wu, B.; Zhang, J.; Theato, P.; Chen, T. Bioinspired Synergistic Fluorescence-Color-Switchable Polymeric Hydrogel Actuators. *Angew. Chem., Int. Ed.* **2019**, *58*, 16243.
(3) Fan, H. L.; Gong, J. P. Fabrication of Bioinspired Hydrogels: Challenges and Opportunities. *Macromolecules* **2020**, *53*, 2769.
(4) Shahsavan, H.; Aghakhani, A.; Zeng, H.; Guo, Y.; Davidson, Z. S.; Priimagi, A.; Sitti, M. Bioinspired Underwater Locomotion of Light-driven Liquid Crystal Gels. *Proc. Natl. Acad. Sci. U.S.A.* **2020**, *117*, 5125.
(5) Wu, S.; Shi, H.; Lu, W.; Wei, S.; Shang, H.; Liu, H.; Si, M.; Le, X.; Yin, G.; Theato, P.; Chen, T. Aggregation-Induced Emissive Carbon Dots Gels for Octopus-Inspired Shape/Color Synergistically Adjustable Actuators. *Angew. Chem., Int. Ed.* **2021**, *60*, 21890.
(6) Li, Z.; Liu, P. C.; Ji, X. F.; Gong, J. Y.; Hu, Y. B.; Wu, W. J.; Wang, X. N.; Peng, H. Q.; Kwok, R. T. K.; Lam, J. W. Y.; et al. Bioinspired Simultaneous Changes in Fluorescence Color, Brightness, and Shape of Hydrogels Enabled by AIEgens. *Adv. Mater.* **2020**, *32*, No. 1906493.
(7) Ma, C.; Lu, W.; Yang, X.; He, J.; Le, X.; Wang, L.; Zhang, J.; Serpe, M. J.; Huang, Y.; Chen, T. Bioinspired Anisotropic Hydrogel Actuators with On-Off Switchable and Color-Tunable Fluorescence Behaviors. *Adv. Funct. Mater.* **2018**, *28*, No. 1704568.
(8) Ji, X. F.; Li, Z.; Hu, Y. B.; Xie, H. L.; Wu, W. J.; Song, F. Y.; Liu, H. X.; Wang, J. G.; Jiang, M. J.; Lam, J. W. Y.; Zhong Tang, B. Bioinspired Hydrogels with Muscle-Like Structure for AIEgen-Guided Selective Self-Healing. *CCS Chem.* **2021**, *3*, 1146.
(9) Ma, Y. F.; Hua, M. T.; Wu, S. W.; Du, Y. J.; Pei, X. W.; Zhu, X. Y.; Zhou, F.; He, X. M. Bioinspired High-power-density Strong Contractile Hydrogel by Programmable Elastic Recoil. *Sci. Adv.* **2020**, *6*, No. eabd2520.
(10) Shi, H.; Wu, S.; Si, M.; Wei, S.; Lin, G.; Liu, H.; Xie, W.; Lu, W.; Chen, T. Cephalopod-Inspired Design of Photomechanically Modulated Display Systems for On-Demand Fluorescent Patterning. *Adv. Mater.* **2022**, *34*, No. 2107452.
(11) Xia, Y. L.; He, Y.; Zhang, F. H.; Liu, Y. J.; Leng, J. S. A Review of Shape Memory Polymers and Composites: Mechanisms, Materials, and Applications. *Adv. Mater.* **2020**, *33*, No. 2000713.
(12) Liu, X.; Yuk, H.; Lin, S.; Parada, G. A.; Tang, T. C.; Tham, E.; de la Fuente-Nunez, C.; Lu, T. K.; Zhao, X. 3D Printing of Living Responsive Materials and Devices. *Adv. Mater.* **2018**, *30*, No. 1704821.
(13) Grigoryan, B.; Paulsen, S. J.; Corbett, D. C.; Sazer, D. W.; Fortin, C. L.; Zaita, A. J.; Greenfield, P. T.; Calafat, N. J.; Gounley, J. P.; Taet, A. H.; et al. Multivascular Networks and Functional Intravascular Topologies within Biocompatible Hydrogels. *Science* **2019**, *364*, 458.
(14) Ni, C.; Chen, D.; Zhang, Y.; Xie, T.; Zhao, Q. Autonomous Shapeshifting Hydrogels via Temporal Programming of Photo-switchable Dynamic Network. *Chem. Mater.* **2021**, *33*, 2046.
(15) Wu, B. Y.; Lu, H. H.; Le, X. X.; Lu, W.; Zhang, J. W.; Théato, P.; Chen, T. Recent Progress in the Shape Deformation of Polymeric Hydrogels from Memory to Actuation. *Chem. Sci.* **2021**, *12*, 6472.
(16) Kempaiah, R.; Nie, Z. H. From nature to synthetic systems: shape transformation in soft materials. *J. Mater. Chem. B* **2014**, *2*, 2357.
(17) Fan, W. X.; Shan, C. Y.; Guo, H. Y.; Sang, J. W.; Wang, R.; Zheng, R. R.; Sui, K. Y.; Nie, Z. H. Dual-gradient Enabled Ultrafast Biomimetic Snapping of Hydrogel Materials. *Sci. Adv.* **2019**, *5*, No. eaav7174.
(18) Jiao, D.; Zhu, Q. L.; Li, C. Y.; Zheng, Q.; Wu, Z. L. Programmable Morphing Hydrogels for Soft Actuators and Robots: From Structure Designs to Active Functions. *Acc. Chem. Res.* **2022**, *55*, 1533.
(19) Zheng, J.; Xiao, P.; Le, X. X.; Lu, W.; Théato, P.; Ma, C. X.; Du, B. Y.; Zhang, J. W.; Huang, Y. J.; Chen, T. Mimosa Inspired Bilayer Hydrogel Actuator Functioning in Multi-environments. *J. Mater. Chem. C* **2018**, *6*, 1320.
(20) Xiao, S. W.; Yang, Y.; Zhong, M. Q.; Chen, H.; Zhang, Y. X.; Yang, J. T.; Zheng, J. Salt-Responsive Bilayer Hydrogels with Pseudo-Double-Network Structure Actuated by Polyelectrolyte and Anti-polyelectrolyte Effects. *ACS Appl. Mater. Interfaces* **2017**, *9*, 20843.
(21) Hao, X. P.; Xu, Z.; Li, C. Y.; Hong, W.; Zheng, Q.; Wu, Z. L. Kirigami-Design-Enabled Hydrogel Multimorphs with Application as a Multistate Switch. *Adv. Mater.* **2020**, *32*, No. 2000781.
(22) Nojoomi, A.; Jeon, J.; Yum, K. 2D Material Programming for 3D Shaping. *Nat. Commun.* **2021**, *12*, No. 603.
(23) Zhu, Q. L.; Dai, C. F.; Wagner, D.; Daab, M.; Hong, W.; Breu, J.; Zheng, Q.; Wu, Z. L. Distributed Electric Field Induces Orientations of Nanosheets to Prepare Hydrogels with Elaborate Ordered Structures and Programmed Deformations. *Adv. Mater.* **2020**, *32*, No. 2005567.
(24) Zhu, Q. L.; Du, C.; Dai, Y. H.; Daab, M.; Matejdes, M.; Breu, J.; Hong, W.; Zheng, Q.; Wu, Z. L. Light-steered Locomotion of Muscle-like Hydrogel by Self-coordinated Shape Change and Friction Modulation. *Nat. Commun.* **2020**, *11*, No. 5166.
(25) Cui, H. L.; Pan, N.; Fan, W. X.; Liu, C. Z.; Li, Y. Y.; Xia, Y. Z.; Sui, K. Y. Ultrafast Fabrication of Gradient Nanoporous All-Polysaccharide Films as Strong, Superfast, and Multiresponsive Actuators. *Adv. Funct. Mater.* **2019**, *29*, No. 1807692.
(26) Tan, Y.; Wang, D.; Xu, H. X.; Yang, Y.; Wang, X. L.; Tian, F.; Xu, P. P.; An, W. L.; Zhao, X.; Xu, S. M. Rapid Recovery Hydrogel Actuators in Air with Bionic Large-Ranged Gradient Structure. *ACS Appl. Mater. Interfaces* **2018**, *10*, 40125.
(27) Sun, Z. F.; Yamauchi, Y.; Araoka, F.; Kim, Y. S.; Bergueiro, J.; Ishida, Y.; Ebina, Y.; Sasaki, T.; Hikima, T.; Aida, T. An Anisotropic Hydrogel Actuator Enabling Earthworm-Like Directed Peristaltic Crawling. *Angew. Chem., Int. Ed.* **2018**, *57*, 15772.
(28) Han, D.; Farino, C.; Yang, C.; Scott, T.; Browe, D.; Choi, W.; Freeman, J. W.; Lee, H. Soft Robotic Manipulation and Locomotion

with a 3D Printed Electroactive Hydrogel. *ACS Appl. Mater. Interfaces* **2018**, *10*, 17512.
(29) Nojoomi, A.; Arslan, H.; Lee, K.; Yum, K. Bioinspired 3D Structures with Programmable Morphologies and Motions. *Nat. Commun.* **2018**, *9*, No. 3705.
(30) Ma, C. X.; Le, X. X.; Tang, X. L.; He, J.; Xiao, P.; Zheng, J.; Xiao, H.; Lu, W.; Zhang, J. W.; Huang, Y. J.; Chen, T. A Multiresponsive Anisotropic Hydrogel with Macroscopic 3D Complex Deformations. *Adv. Funct. Mater.* **2016**, *26*, 8670.
(31) Xiao, S. W.; Zhang, M. Z.; He, X. M.; Huang, L.; Zhang, Y. X.; Ren, B. P.; Zhong, M. Q.; Chang, Y.; Yang, J. T.; Zheng, J. Dual Salt- and Thermoresponsive Programmable Bilayer Hydrogel Actuators with Pseudo-Interpenetrating Double-Network Structures. *ACS Appl. Mater. Interfaces* **2018**, *10*, 21642.
(32) Kim, S. Y.; Baines, R.; Booth, J.; Vasios, N.; Bertoldi, K.; Kramer-Bottiglio, R. Reconfigurable soft body trajectories using unidirectionally stretchable composite laminae. *Nat. Commun.* **2019**, *10*, No. 3464.
(33) Li, T. Z.; Wang, J. H.; Zhang, L. Y.; Yang, J. B.; Yang, M. Y.; Zhu, D. Y.; Zhou, X. H.; Handschuh-Wang, S.; Liu, Y. Z.; Zhou, X. C. "Freezing", Morphing, and Folding of Stretchy Tough Hydrogels. *J. Mater. Chem. B* **2017**, *5*, 5726.
(34) Luan, H.; Cheng, X.; Wang, A.; Zhao, S.; Bai, K.; Wang, H.; Pang, W.; Xie, Z.; Li, K.; Zhang, F.; et al. Design and Fabrication of Heterogeneous, Deformable Substrates for the Mechanically Guided 3D Assembly. *ACS Appl. Mater. Interfaces* **2019**, *11*, 3482.
(35) Song, S. W.; Lee, S.; Choe, J. K.; Kim, N. H.; Kang, J.; Lee, A. C.; Choi, Y.; Choi, A.; Jeong, Y.; Leeet, W.; et al. Direct 2D-to-3D Transformation of Pen Drawings. *Sci. Adv.* **2021**, *7*, No. eabf3804.
(36) Tang, L.; Wang, L.; Yang, X.; Feng, Y.; Li, Y.; Feng, W. Poly(*N*-isopropylacrylamide)-based Smart Hydrogels: Design, Properties and Applications. *Prog. Mater Sci.* **2021**, *115*, No. 100702.
(37) Zheng, W. J.; An, N.; Yang, J. H.; Zhou, J. X.; Chen, Y. M. Tough Al-alginate/poly(N-isopropylacrylamide) hydrogel with tunable LCST for soft robotics. *ACS Appl. Mater. Interfaces* **2015**, *7*, 1758.
(38) Yao, C.; Liu, Z.; Yang, C.; Wang, W.; Ju, X. J.; Xie, R.; Chu, L. Y. Poly(*N*-isopropylacrylamide)-Clay Nanocomposite Hydrogels with Responsive Bending Property as Temperature-Controlled Manipulators. *Adv. Funct. Mater.* **2015**, *25*, 2980.
(39) Peng, X.; Liu, T.; Jiao, C.; Wu, Y.; Chen, N.; Wang, H. Complex Shape Deformations of Homogeneous Poly(*N*-isopropylacrylamide)/graphene Oxide Hydrogels Programmed by Local NIR Irradiation. *J. Mater. Chem. B* **2017**, *5*, 7997.
(40) Zheng, Y.; Cheng, Y.; Chen, J.; Ding, J.; Li, M.; Li, C.; Wang, J. C.; Chen, X. Injectable Hydrogel-Microsphere Construct with Sequential Degradation for Locally Synergistic Chemotherapy. *ACS Appl. Mater. Interfaces* **2017**, *9*, 3487.
(41) Del Monte, G.; Truzzolillo, D.; Camerin, F.; Ninarello, A.; Chauveau, E.; Tavagnacco, L.; Gnan, N.; Rovigatti, L.; Sennato, S.; Zaccarelli, E. Two-step Deswelling in the Volume Phase Transition of Thermoresponsive Microgels. *Proc. Natl. Acad. Sci. U.S.A.* **2021**, *118*, No. e2109560118.
(42) Jian, Y. K.; Wu, B. Y.; Yang, X. X.; Peng, Y.; Zhang, D. C.; Yang, Y.; Qiu, H. Y.; Lu, H. H.; Zhang, J. W.; Chen, T. Stimuli-responsive Hydrogel Sponge for Ultrafast Responsive Actuator. *Supramol. Mater.* **2022**, *1*, No. 100002.
(43) Zhang, T.; Xu, Z.; Gui, H.; Guo, Q. Emulsion-templated, Macroporous Hydrogels for Enhancing Water Efficiency in Fighting Fires. *J. Mater. Chem. A* **2017**, *5*, 10161.
(44) Wu, B. Y.; Lu, H. H.; Jian, Y. K.; Zhang, D. C.; Peng, Y.; Zhuo, J.; Le, X. X.; Zhang, J. W.; Théato, P.; Chen, T. Interfacial Reinitiation of Free Radicals Enables the Reborn of Broken Polymeric Hydrogel Actuators. *CCS Chem.* **2022**, 1−14, DOI: 10.31635/ccschem.022.202201942.
(45) Witte, J.; Kyrey, T.; Lutzki, J.; Dahl, A. M.; Houston, J.; Radulescu, A.; Pipich, V.; Stingaciu, L.; Kuhnhammer, M.; Witt, M. U.; et al. A Comparison of the Network Structure and Inner Dynamics of Homogeneously and Heterogeneously Crosslinked PNIPAm Microgels with High Crosslinker Content. *Soft Matter* **2019**, *15*, 1053.
(46) Park, N.; Kim, J. Hydrogel-Based Artificial Muscles: Overview and Recent Progress. *Adv. Intell. Syst.* **2020**, *2*, No. 1900135.
(47) Lin, H.; Ma, S.; Yu, B.; Cai, M.; Zheng, Z. J.; Zhou, F.; Liu, W. Fabrication of Asymmetric Tubular Hydrogels through Polymerization-Assisted Welding for Thermal Flow Actuated Artificial Muscles. *Chem. Mater.* **2019**, *31*, 4469.
(48) Wang, L.; Jian, Y. K.; Le, X. X.; Lu, W.; Ma, C. X.; Zhang, J. W.; Huang, Y. J.; Huang, C. F.; Chen, T. Actuating and Memorizing Bilayer Hydrogels for a Self-deformed Shape memory Function. *Chem. Commun.* **2018**, *54*, 1229.
(49) Lu, W.; Le, X. X.; Zhang, J. W.; Huang, Y. J.; Chen, T. Supramolecular shape memory hydrogels: a new bridge between stimuli-responsive polymers and supramolecular chemistry. *Chem. Soc. Rev.* **2017**, *46*, 1284.
(50) Le, X.; Lu, W.; Zheng, J.; Tong, D.; Zhao, N.; Ma, C.; Xiao, H.; Zhang, J.; Huang, Y.; Chen, T. Stretchable supramolecular hydrogels with triple shape memory effect. *Chem. Sci.* **2016**, *7*, 6715.
(51) Sun, J. Y.; Zhao, X.; Illeperuma, W. R.; Chaudhuri, O.; Oh, K. H.; Mooney, D. J.; Vlassak, J. J.; Suo, Z. Highly Stretchable and Tough Hydrogels. *Nature* **2012**, *489*, 133.
(52) Ma, C. X.; Li, T. F.; Zhao, Q.; Yang, X. X.; Wu, J. J.; Luo, Y. W.; Xie, T. Supramolecular Lego Assembly towards Three-dimensional Multi-responsive Hydrogels. *Adv. Mater.* **2014**, *26*, 5665.
(53) Wu, B. Y.; Xu, Y. W.; Le, X. X.; Jian, Y. K.; Lu, W.; Zhang, J. W.; Chen, T. Smart Hydrogel Actuators Assembled via Dynamic Boronic Ester Bonds. *Acta Polym. Sin.* **2019**, *50*, 496.
(54) Ge, Q.; Chen, Z.; Cheng, J. X.; Zhang, B.; Zhang, Y. F.; Li, H. G.; He, X. N.; Yuan, C.; Liu, J.; Magdassiet, S.; Qu, S. 3D Printing of Highly Stretchable Hydrogel with Diverse UV Curable Polymers. *Sci. Adv.* **2021**, *7*, No. eaba4261.